Environmental Earth Sciences (2020) 79:362
https://doi.org/10.1007/s12665-020-09106-z

ORIGINAL ARTICLE

Evaluation of infilling and replenishment of river sand mining pits

Hamed Haghnazar[1] · Yousef Sangsefidi[2] · Mojtaba Mehraein[3] · Hassan Tavakol-Davani[2]

Received: 18 March 2020 / Accepted: 2 July 2020 / Published online: 11 July 2020

Abstract
Rivers are one of the main sources to supply sand and gravel for construction projects. Depending on river morphology and hydraulic characteristics, its sediment transport capacity, and mining operation method, the extraction of river bed materials may affect its ecosystem through bank and bed erosion. To advance the mechanisms of river pit infilling, the effects of various parameters (i.e., the distance between pits, the pit plan shape, the pit depth, sediment size, and approaching flow velocity) on pit infilling volume are investigated in this research. The results of this research show that infilling volume of upstream pit is insignificantly affected by the distance between the pits, and it is completely refilled for different distances. However, the infilling volume of downstream pit decreases by increasing the distance between the pits. In addition, by reducing the ratio of pit length to its width (pit shape extension in spanwise direction), the pits can be excavated in a shorter distance from each other; when this ratio decreases by 15%, the infilling volume increases up to 30%. Subsequently, as a cost-effective option, the pit distance can be reduced up to 50% in these conditions. According to the obtained results, although the sediment size has negligible effect on infilling volume in the studied range, the infilling volume increases up to 20% by an increase of 8% in the approaching flow velocity. Increasing the ratio of pit length to its width (pit shape extension in streamwise direction) highlights the effectiveness of smaller depths, so that the infilling volume increases up to 20% by a decrease of 20% in the pit depth. In this regard, it is recommended that the pit depth be restricted to 70% of the channel flow depth to have a complete pit refilling.

Keywords Sand mining · Pit infilling · River bed material · Morphology

Introduction

One of the key parameters affecting the final cost, duration, and quality of construction projects is providing the appropriate material. Due to easy access, river sand and gravel have been used extensively in construction projects. Depending on the mining operation method as well as hydraulic and morphologic characteristics of the river, sand mining may cause bed and bank erosion or other negative consequences for the river ecosystem. Therefore, it is necessary to conduct appropriate studies to explore sustainable and cost-effective methods for river mining.

✉ Mojtaba Mehraein
mehraein@khu.ac.ir

1 Department of Civil Engineering, Shahrood University of Technology, Shahrood, Iran

2 Urban Water Group, San Diego State University, San Diego, CA, USA

3 Faculty of Engineering, Kharazmi University, Tehran, Iran

Some effects of sand mining on river mechanisms have been evaluated in the different series of field, experimental, and numerical studies. According to previous field studies, in the nickpoint (attachment region of the sediment bed and the pit), the bed slope increases suddenly. This is known as the head cutting process, in which an erodible region moves upstream (Collins and Dunne 1989; Surian and Rinaldi 2003; Marston et al. 2003). In addition, as the flow passes the downstream edge of the pit, the hydraulic flow condition and channel geometry tend to the ones in the upstream of pit. Hence, the sediment transport capacity of the flow increases; as a result, erosion will occur in the downstream region. In the other hand, the sediments deposition (occurred inside the pits and in their edges) makes hungry water, which increases the sediment transport capacity of the flow. (Rinaldi and Simon 1998; Kondolf 1997; Erskine et al. 1990). Downstream river bank heights are thereby increased, which threats the river through its bank collapse (Sreebha and Padmalal 2011; Padmalal et al. 2008; Rinaldi 2003; Batalla 2003). According to Erskine et al. (1985), the river bed material mining decreases the thickness of the large-sized sediments bed layer (thinning of armor layer), and, subsequently, increases the bed erosion. The pit proximity and merging (due to upstream and downstream erosion) decreases the sediment bed elevation (Calle et al. 2017; Padmalal et al. 2008) and changes the bed and suspended loads (Ferguson et al. 2015; Bayram and Önsoy 2015; Ashraf et al. 2011). In addition, an excess river material mining affects insects and invertebrates, which breed in aquatic environments (Padmalal and Maya 2014). Sunilkumar (2002) showed that sand and gravel mining impacts aquatic organisms severely as it destroys the spawning area and food source for fish (Padmalal and Maya 2014; Ambak and Zakaria 2010). In addition, sediment reduces the river water quality by increasing the concentration of the heavy metals and decreasing water transparency (Bayram and Önsoy 2015).

A series of laboratory experiments have been also conducted to determine the effects of different parameters on the pit migration velocity. According to Lee et al. (1993), pit deformation and migration include two periods. In the first period (convection period), the upstream slope of the pit gradually moves in streamwise direction and reaches the downstream slope of the pit. However, the maximum depth of the pit is almost constant during this period. In the second period (diffusion period), the pit depth decreases during the time, so that the pit eventually fills by sediments. Sediments are deposited in the pit, which migrates downstream with constant slope. Thus, increasing the migration velocity improves the pit filling rate (Jang et al., 2015). According to Barman et al. (2017) and Li et al. (2013), upstream edge erosion is less than the downstream edge as the bed load causes the pit to migrate downstream. In addition, the pit migration velocity depends on its geometry (length and width). The effect of the pit length on pit migration speed is more significant than that of pit width (Yuill et al. 2016; Salehi Neishabouri et al. 2002). Recently, Haghnazar and Saneie (2019) experimentally investigated the effects of distance between pits for $l/b = 1.28$.

With recent significant advances in Computational Fluid Dynamics (CFD) algorithms and computing power, various numerical packages (e.g., CCHE2D and HEC-RAS software) have been applied to simulate the flow features and sedimentation transport around river pits. Chen et al. (2010), for example, stated that in the simulation of flood and river geomorphology variations, CCHE2D gives better results as compared to HEC-RAS. According to Chen and Liu (2009), HEC-RAS overestimates the head cutting due to the presence of some errors in the velocity prediction in the upstream section of the pit. Using CCHE2D, they also found that the streamlines of passing flow approach to the pit upstream corners, and then, obviate from its downstream corners; this phenomenon can dramatically change the flow structure. This software package presents downstream pit erosion and sediment deposition in the pit upstream edge in more detail. Chen (2011) used Lee et al.'s (1993) experimental data along with CCHE2D software to simulate flow structure in the presence of a mining pit. The results showed that the software can predict the ensuing bed change with acceptable accuracy (having $R^2 = 0.77$).

The conducted literature review shows that the assessment of behavioral differences between a single pit and a pair of pits, the effects of pit plan shape, the interaction of plan shape with the distance between pits, and the capability of numerical models in describing river tow-pit behavior merit more investigations. In this study, the effects of different parameters (including the distance between the pits, the pit plan shape, the pit depth, sediment size, and approaching flow velocity) on the pit infilling and replenishment process are investigated using both experimental models and numerical simulations (conducted by CCHE2D). The specific objectives of the present study are:

- to evaluate the ability of CCHE2D software in predicting the pit infilling process (using a comparison with the collected experimental data);
- to gain new insights about flow behavior and sediment transport around river pits (based on both experimental and numerical models); and
- to propose practical recommendations for the extraction method of river bed material.

Materials and methods

To gain new insights about flow features and sediment transport around river mining pits, the effects of five dimensionless parameters on the pit infilling and replenishment processes are investigated in this study. These parameters include the ratio of the distance between pits to approaching flow depth (L/y), the ratio of pit length to its width (l/b), the ratio of pit depth to approaching flow depth (H/y), the ratio of median sediment size to approaching flow depth (d_{50}/y), and the ratio of approaching flow velocity to sediment critical velocity (U/U_c). In the experimental tests, the effects of L/y are investigated, while other parameters are kept constant. The effects of other above-mentioned parameters are investigated using numerical simulations. In addition, the results of laboratory experiments are used to verify the numerical simulations.

Experimental method

Experimental setup characteristics

Experiments were conducted in a recirculating laboratory channel with 14 m length, 1.5 m width, and 0.5 m height. A schematic view of the channel along with the mining pits is

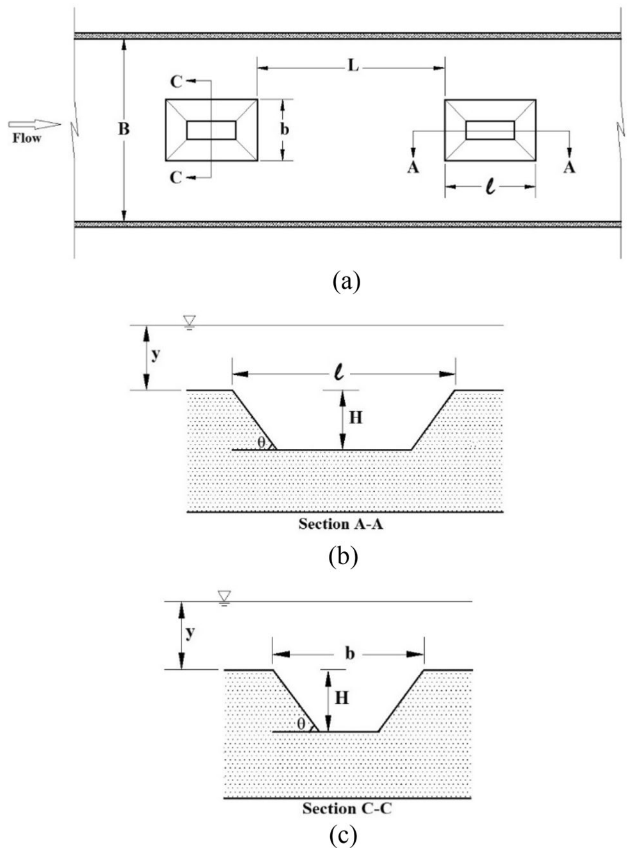

Fig. 1 A schematic view of the channel: **a** plan view; **b** section view A–A; **c** section view C–C

Fig. 2 Metal molds for the formation of mining pits

presented in Fig. 1. Before each experiment, the sediment bed was leveled, and the metal molds were located in given positions to form mining pits (Fig. 2). The initial volume and side wall slope of all mining pits were set to V_0= 6515 cm^3 and $\theta = 30.7°$, respectively. In all experiments, the length, width, and depth of the mining pits were, respectively, considered as 46, 36, and 9.5 cm (corresponding to the fixed value of $l/b = 1.28$).

Relatively uniform sediments with $d_{50} = 1$ mm and $\sigma_g = (d_{84}/d_{16})^{0.5} = 1.46$ are used as sediment bed material (d_i = the diameter that is larger than the diameter of i percent of sediments by weight; σ_g = the standard deviation of the sediment diameters). In all experiments, the sediment layer thickness and flow depth were 15 and 6 cm, respectively. According to Sangsefidi et al. (2020), viscosity effects are insignificant at high enough Reynolds number in which the flow is turbulent. In addition, in Froude-scaled models, the surface tension effects are negligible when the flow depth is greater than 0.025 m. According to Table 1, these recommendations have been satisfied for all the conducted experiments (having $\text{Re} = \rho U y/\mu = 22896$ and $y = 6$ cm).

Infilling tests

In the present research, the sediment bed critical velocity (U_c) is determined empirically, since there are some discrepancies among existing formulas in the literature for evaluating this parameter. At the beginning of experiments, the sediment bed was leveled, and the flow depth was regulated (set to 6 cm) using a downstream gate; then, the flow discharge was increased gradually. According to the experimental observations, the sediment movement starts when flow discharge reaches $Q = 28.62$ l/s (corresponding to $U_c = 0.318$ m/s). While $U/U_c = 1.2$ in all experiments, different values of U/U_c (= 1.15, 1.2, and 1.25) were considered in numerical simulations to evaluate the effects of this parameter on the pit infilling volume.

At the beginning of each test, a very low discharge was released to prevent sediment transport commencing immediately. According to the test procedure, when the channel was submerged, the discharge was increased gradually to reach the desired value while the flow depth was regulated to 6 cm. Then, by removing metal molds from the channel bed, the test was started. The test was completed after 1 h, and then, the channel was drained for doing the measurements.

Table 1 Experimental details

Exp. no.	Pit numbers	L/y	l/b	H/y	d_{50}/y	U/U_c
1	1	–	1.28	1.59	0.016	1.2
2	2	8	1.28	1.59	0.016	1.2
3	2	12	1.28	1.59	0.016	1.2
4	2	16	1.28	1.59	0.016	1.2

To determine the bed topography around the pits, the sediment bed levels were measured at 285 different points using a point gauge (having ± 0.1 mm accuracy).

Flow velocity test

In one experiment (mentioned in Table 2), the longitudinal and transverse components of mean velocities were measured using a 2D electromagnetic velocimeter. To prevent the bed material from movement, the flow depth was set to $y = 11$ cm in flow velocity tests ($y = 6$ cm in the infilling tests having movable bed materials). The flow velocities were measured at 384 different points at $z = 6.6$ cm. A calibrated rectangular weir and the mentioned point gauge were used to measure flow discharges and depths, respectively.

Numerical method

CCHE2D software package

In this study, CCHE2D software (as a two-dimensional depth-averaged CFD package) is used to simulate flow characteristics and sediment transport process around river pits. This software solves the depth-averaged RANS equations using the finite-element method (Papanicolaou et al. 2008). In addition, the models of parabolic eddy viscosity, mixing length, or k–ε can be used for turbulence closure. The sediment transport model of the software can simulate the bed and suspended loads in both steady and unsteady conditions considering cohesive and non-cohesive sediments.

Governing equations

According to Zhang (2005), In Cartesian coordinates, the depth-averaged momentum and continuity equations for a turbulent flow can be expressed as:

$$\frac{\partial Z}{\partial t} + \frac{\partial (hu)}{\partial x} + \frac{\partial (hv)}{\partial y} = 0 \tag{1}$$

$$\frac{\partial u}{\partial t} + u\frac{\partial u}{\partial x} + v\frac{\partial u}{\partial y} = -g\frac{\partial Z}{\partial x} + \frac{1}{h}\left(\frac{\partial h\tau_{xx}}{\partial x} + \frac{\partial h\tau_{xy}}{\partial y}\right) - \frac{\tau_{bx}}{\rho h} + f_{\text{cor}}v \tag{2}$$

$$\frac{\partial v}{\partial t} + u\frac{\partial v}{\partial x} + v\frac{\partial v}{\partial y} = -g\frac{\partial Z}{\partial y} + \frac{1}{h}\left(\frac{\partial h\tau_{yx}}{\partial x} + \frac{\partial h\tau_{yy}}{\partial y}\right) - \frac{\tau_{by}}{\rho h} + f_{\text{cor}}u, \tag{3}$$

where t = time, u and v = depth-averaged streamwise and spanwise velocity components, g = gravity acceleration, z = water surface level, ρ = flow density, h = local flow depth, f_{cor} = Coriolis acceleration coefficient, τ_{xy}, τ_{xx}, τ_{yy}, and τ_{yx} = depth-averaged Reynolds stress components, τ_{bx} = shear bed stress in x direction, and τ_{by} = shear bed stress in y direction. The convection–diffusion equation of K and ε are expressed in Eqs. (4) and (5):

$$\frac{\partial (\rho K)}{\partial t} + \frac{\partial (\rho K u_i)}{\partial x_i} = \frac{\partial}{\partial x_j}\left[\left(\mu + \frac{\mu_t}{\sigma_k}\right)\frac{\partial K}{\partial x_j}\right] + G - \rho\varepsilon \tag{4}$$

$$\frac{\partial (\rho \varepsilon)}{\partial t} + \frac{\partial (\rho \varepsilon u_i)}{\partial x_i} = \frac{\partial}{\partial x_j}\left[\left(\mu + \frac{\mu_t}{\sigma_\varepsilon}\right)\frac{\partial \varepsilon}{\partial x_j}\right] + C_{1_\varepsilon}\frac{\varepsilon}{K}G - C^*_{2_\varepsilon}\rho\frac{\varepsilon^2}{K}G, \tag{5}$$

where μ_t = turbulent viscosity and G = energy turbulent generation; and they can be determined by the following equations:

$$\mu_t = \rho C_\mu \frac{K^2}{\varepsilon} \tag{6}$$

$$G = \mu_t\left(\frac{\partial u_i}{\partial x_j} + \frac{\partial u_j}{\partial x_i}\right)\frac{\partial u_i}{\partial x_j}. \tag{7}$$

In addition, we have Eq. (8) for the parameter $C^*_{2_\varepsilon}$:

$$C^*_{2_\varepsilon} = C_{2_\varepsilon} + \frac{C_\mu \eta^3 (1 - \eta/\eta_0)}{1 + \beta\eta^3}, \quad \eta = \frac{SK}{\varepsilon}, \quad S = (2S_{ij}S_{ij})^{0.5}, \quad S_{ij} = \frac{1}{2}(u_{ij}u_{ji}). \tag{8}$$

According to Wu (2001), the sediment transport models for the bed and suspended loads are based on the continuity and depth-averaged convection–diffusion equations, respectively, as follows:

$$(1 - p')\frac{\partial Z_{bk}}{\partial t} + \frac{\partial (\delta c_{bk})}{\partial t} + \frac{\partial q_{bkx}}{\partial x} + \frac{\partial q_{bky}}{\partial y} = -E_{bk} + D_{bk}, (k = 1, 2, \ldots, N) \tag{9}$$

$$\frac{\partial (hC_k)}{\partial t} + \frac{\partial (UhC_k)}{\partial x} + \frac{\partial (VhC_k)}{\partial y} = \frac{\partial}{\partial x}\left(\varepsilon_s h\frac{\partial C_k}{\partial x}\right) + \frac{\partial}{\partial y}\left(\varepsilon_s h\frac{\partial C_k}{\partial y}\right) + E_{bk} - D_{bk}, \tag{10}$$

Table 2 Details of the flow measurement experiment

Flow depth (cm)	Flow discharge (l/s)	Pit numbers	L/y	l/b	H/y	d_{50}/y
11	28.62	2	12	1.28	1.59	0.016

where k = sediment size class, p' = porosity of the sediment bed, c_{bk} = bed load sediment concentration in the bed load region, = thickness of the bed load layer, q_{bkx} and q_{bky} = rate of sediment bed load in x and y directions, Z_b = bed elevation, C_k = suspended sediment concentration, and ε_s = sediment eddy diffusivity, which can be determined by:

$$\varepsilon_{\mathrm{s}} = \frac{\upsilon_{\mathrm{t}}}{\sigma_{\mathrm{s}}}, \tag{11}$$

where υ_{t} = kinematic eddy viscosity (or the turbulent diffusion coefficient of momentum of clear water flow) and σ_{s} = Schmidt–Ptantle number. Also, E_{bk} = the sediment transport rate from the bed load region to the suspended load region and D_{bk} = the sediment deposition rate at the interface between the bed load region and suspended load region. We have:

$$E_{bk} - D_{bk} = \alpha\omega_{sk}\left(C_{*k} - C_k\right), \tag{12}$$

where α = the nonequilibrium adaption coefficient for suspended load, ω_{sk} = the terminal fall velocity of the sediment size class, and C_{*k} = the sediment concentration in equilibrium condition (sediment capacity).

Numerical simulation of flow field and sediment transport

At the first step of the numerical simulation, flow field is simulated, and then, the sediment transport simulation is conducted based on the simulated flow field. According to Table 3, three different mesh sizes were used to evaluate the effect of the mesh size on the results.

The inlet (having a specific discharge) and outlet (having a specific flow depth) boundary conditions were applied in the upstream and downstream sections, respectively. A solid wall was used as the boundary condition for the channel side walls (Sangsefidi et al. 2019). However, an erodible bed was considered for the bottom boundary. The roughness coefficient was applied using the Strickler (1923) equation, and $K-\varepsilon$ model was employed for turbulence closure. The other characteristics of the numerical models (i.e., median sediment size, bed roughness coefficient, sediment-specific gravity, bed layer thickness, and simulations time) are presented in Table 4.

Table 3 Different mesh characteristics

Mesh name	Cell dimensions (cm)
M-0.5-0.5	0.5×0.5
M-1-1	1×1
M-2-2	2×2

Results and discussion

Upstream pit (Pit A)

The effects of the distance between pits are evaluated by considering different values of L/y = 0, 8, 12, and 16 while l/b = 1.28, d_{50}/y = 0.016, H/y = 1.59, and U/U_{c} = 1.2. At the beginning of the experiments, the sediments mobilize from upstream sections and deposit near the pit upstream edge. This process forces the pit upstream slope to move toward the downstream, and the pit depth decreases. In addition, at this stage of the experiments, by eroding the downstream edge of the pit, the sediment moves in streamwise direction toward the downstream sections. After excavating mining pits, the flow velocity decreases in this location; thus, sediment can fall and deposit into the pit. As a result, the erosion capacity of passing flow increases in the downstream of the pit. Figure 3a–c illustrates the longitudinal bed profiles in the centerline of upstream pit (pit A) for different values of L/y. Figure 3d presents a single pit infilling for making a comparison. From Fig. 3, as expected, the pit bed level rises with respect to the time. However, at a given time, the longitudinal bed profiles in pit A are approximately the same for different distances between the pits. These profiles are also similar to that of the single pit. Hence, the effects of downstream pit (pit B) on the behavior of pit A can be neglected.

Figure 4a–c shows the sediment bed topography around pit A for L/y = 8, 12, and 16 at t = 3600 s. Figure 4d also presents the bed topography around the single pit for a comparison. Since the sediment deposition rate on the pit upstream corners is more than that of the upstream edge middle part, their shapes change from sharp corners to round ones. The

Table 4 Details of the parameters used in sediment transport modeling

Numerical simulation			Median sediment size (mm)	Bed roughness coefficient (m)	Sediment-specific gravity (kg/m^3)	Bed layer thickness (cm)	Simulation time (s)
Sediment size effects	Other parameter effects	Verification					
■	■	■	1	0.0150	2650	15	3600
■	□	□	0.8	0.0144	2650	15	3600
■	□	□	0.6	0.0138	2650	15	3600

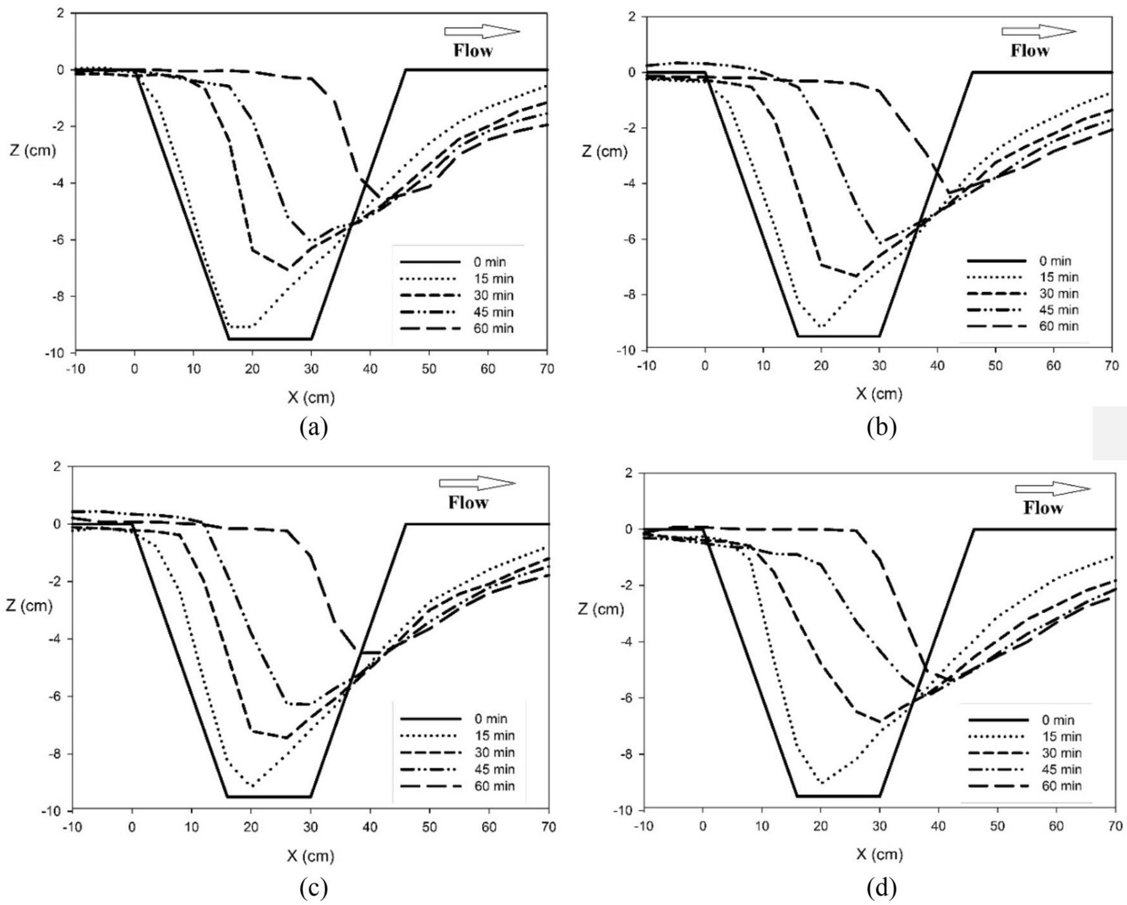

Fig. 3 Longitudinal bed profiles in the centerline of pit A for *L*/*y* = **a** 8; **b** 12; **c** 16; **d**) 0 (single pit)

deposition and erosion processes occur near the upstream and downstream edges of the pit, respectively. In addition, based on qualitative comparisons, the shape of pit A does not change significantly in different *L*/*y* values; thus, the effects of the distance (or existence) of pit B on the deposition and erosion processes of pit A are negligible.

Downstream pit (Pit B)

Figure 5a–c shows the longitudinal bed profiles in the centerline of pit B with respect to time for different values of *L*/*y* when *l*/*b* = 1.28. Figure 5d is also presented for the single pit experiment. As shown, sediment deposition decreases by an increase in *L*/*y* indicating pit A influence on pit B behavior. This is because at smaller values of *L*/*y*, the eroded sediment transports from pit A to pit B in a shorter time. For large values of *L*/*y*, the process of bed load sediment transport has the main contribution in infilling process of the downstream pit. This is because the eroded sediment from the upstream pit mostly deposits at the distance between the pits, and it cannot reach downstream pit to contribute in its infilling process. Consequently, one can conclude that at large values of *L*/*y*, the infilling process of the downstream pit tends to the single pit infilling process.

In Fig. 6, the sediment bed topography around pit B is presented for $t = 3600$ s and different *L*/*y* values. According to the laboratory observations, the transported sediment diverges from the two sides of the pit. Therefore, the sediment erosion occurs across the entire channel width, and the sediment transport region expands, which is in agreement with Barman et al.'s (2018) results. In addition, pit B receives less sediment by getting away from pit A (higher distance between the upstream and downstream pits). Table 5 shows the infilling volume (%) of pits A and B for different *L*/*y* values ($t = 3600$ s). From this table, the distance of pit B has no significant effect on the infilling volume of pit A. However, the infilling volume of pit B increases through approaching to pit A. It is worth noting that as the pits get away from each other, the infilling volume of pit B approaches to that of the single pit (≈ 85%).

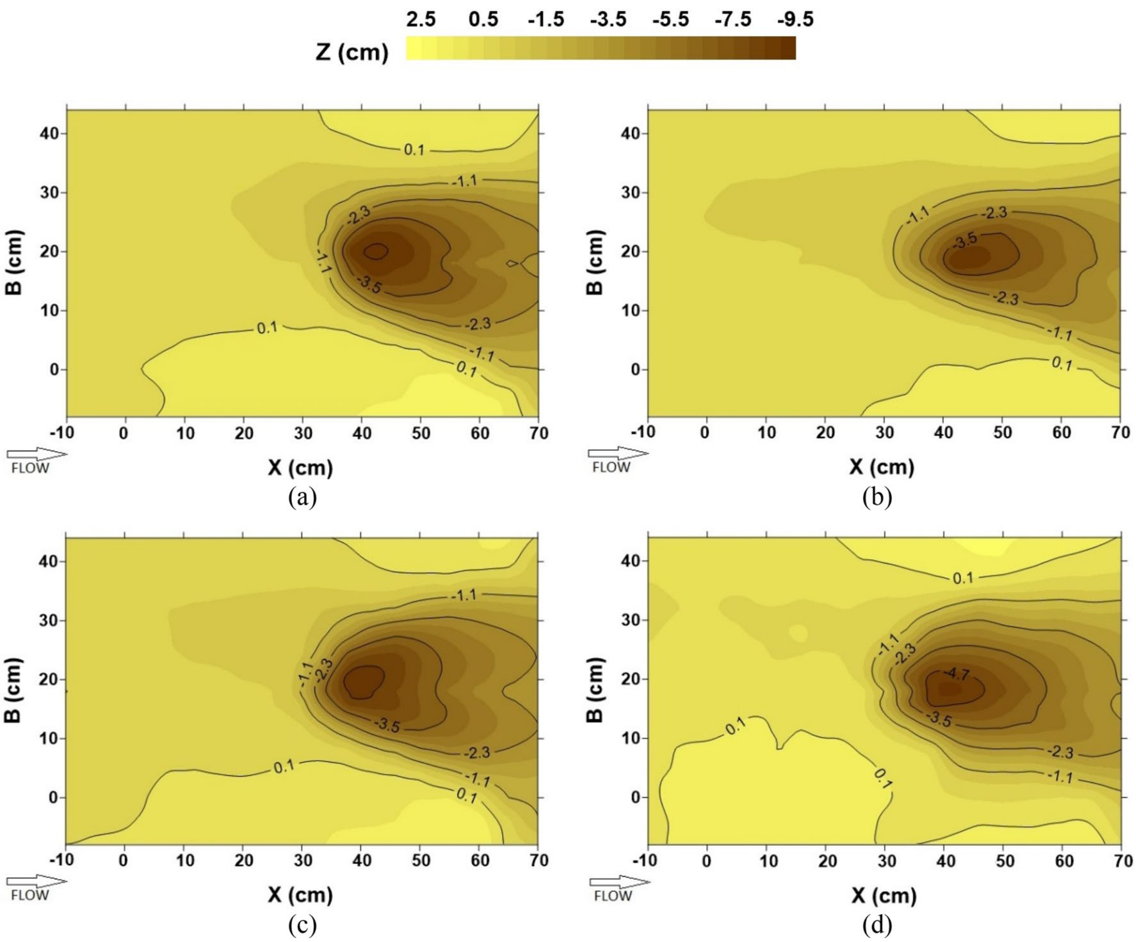

Fig. 4 Bed topography around pit A for *L*/*y* = **a** 8; **b** 12; **c** 16; **d** 0 (single pit)

Verification and evaluation of the numerical model

Figure 7a shows the effects of the simulation time on mean flow velocity in the centerline of the pits. Since the velocity variations are almost the same for $t = 200$ and 300 s, the time duration was set to 200 s in the numerical simulations. The sensitivity analysis of the mesh size, presented in Fig. 7b, shows that the mean flow velocities are almost the same for M-1-1 and M-0.5-0.5 (having an averaged difference of less than 1%). Hence, M-1-1 was selected as the appropriate mesh size in all numerical simulations.

Figure 8 shows the mean velocity contours in streamwise and spanwise directions from numerical and experimental results. In the upstream and downstream edges of the mining pit, the streamwise component of mean velocity increases due to the local reduction in flow depth. However, the streamwise velocity decreases inside the mining pit as the flow depth increases due to the pit presence. The contours of spanwise component of mean velocity show that the flow converges at the upstream corner of the mining pit, while a flow divergence occurs from its downstream corner. Figure 9 shows comparisons between the streamwise and spanwise components of mean velocity in different longitudinal sections. The mean absolute error is 8.72%, and the determination coefficient (R^2) is 0.82 between the experimental and numerical data. Hence, it can be concluded that the numerical simulations have an acceptable accuracy.

Different sediment transport models such as Wu et al.'s (2000) formula, modified Ackers and White's formula (Proffitt and Sutherland 1983), SEDTRA module (Garbrecht et al. 1995), and modified Engelund and Hansen's formula (Wu and Vieira 2000) were used to evaluate the capability of the numerical model in determination of the sediment transport process. The infilling volume is considered as an index to determine the numerical model accuracy. The numerical and experimental results are presented in Table 6 (having $l/b = 1.28$ and $L/y = 16$). From this table, Wu et al.'s (2000) formula has the most agreement with the measured experimental data; thus, it was chosen as the appropriate sediment transport model in the conducted simulations.

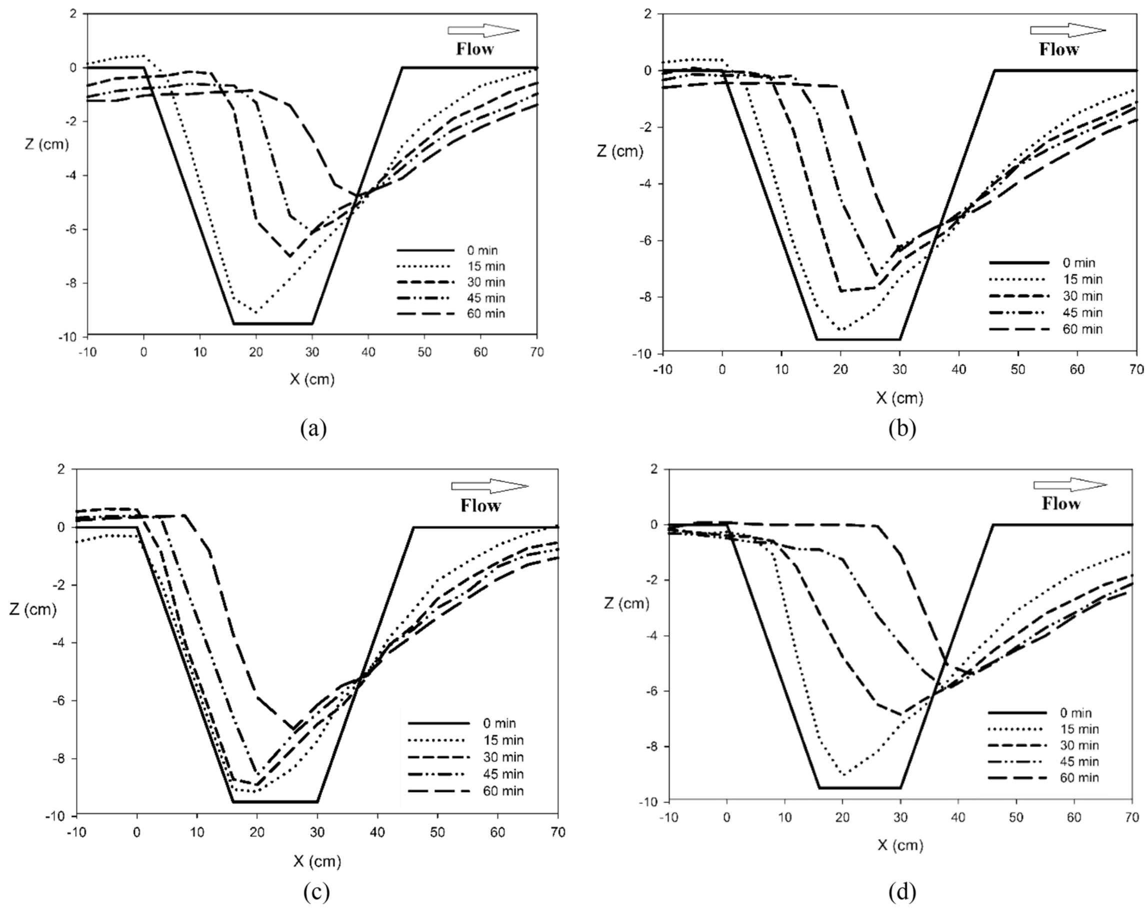

Fig. 5 Longitudinal bed profiles in the centerline of pit B for $L/y=$ **a** 8; **b** 12; **c** 16; **d** 0 (single pit)

Previous studies such as Scott and Jia (2005) and Plesiński et al. (2015) also reported that CCHE2D overestimates the deposition process, which is in agreement with the present study results. They emphasized that the disparity of the obtained results most likely reflects some simplifications at defining boundary conditions in CCHE2D model. It is worth noting that by considering the 2D depth-averaged scheme of CCHE2D, the mentioned differences in results are highly acceptable, especially for describing a complex 3D flow. Figure 10 demonstrates the experimental and numerical results of the sediment bed topography around pits A and B. Using Wu et al.'s (2000) formula, the sediment deposition on the pit sides is larger compared to the experimental results; therefore, the simulated pit is longer and narrower.

It is shown that the velocity profile in numerical simulation is underestimated at $B=0$. It should be noted that although a 3D flow field occurs in the presence of the pits, CCHE2D uses the 2D depth-averaged formulation, which may be the source of the occurred error in the numerical simulation (underestimating the velocity in Fig. 9a). The underestimation of the velocity in the numerical simulation causes that the transported sediment from the upstream region of the pit settles on the pit edge (sediment deposition of Fig. 11a). The accumulated sediment falls into the pit as the height of the accumulated sediment increases, and its slope reaches the critical value. The collapse of the accumulated sediment, therefore, increases the pit infilling volume in the numerical simulations. In addition, the pit bed elevation is higher in the laboratory tests, which is due to the collapse of the pit downstream slope at the beginning of the experiments.

Figure 12 compares the infilling volume in the numerical simulations and the laboratory tests. From this figure, the numerical model has an acceptable accuracy in simulating the pit infilling volume (with an averaged error of 11.9%).

Effects of pit plan shape

As shown in Fig. 13, the effects of pit plan shape were evaluated by considering different values for the parameter l/b (=0.59, 0.78, 1.28, and 1.68). At the beginning of the numerical simulations, all mining pit geometries had a same volume. At this section, only the single pit was simulated to evaluate the effect of pit plan shape on its infilling volume,

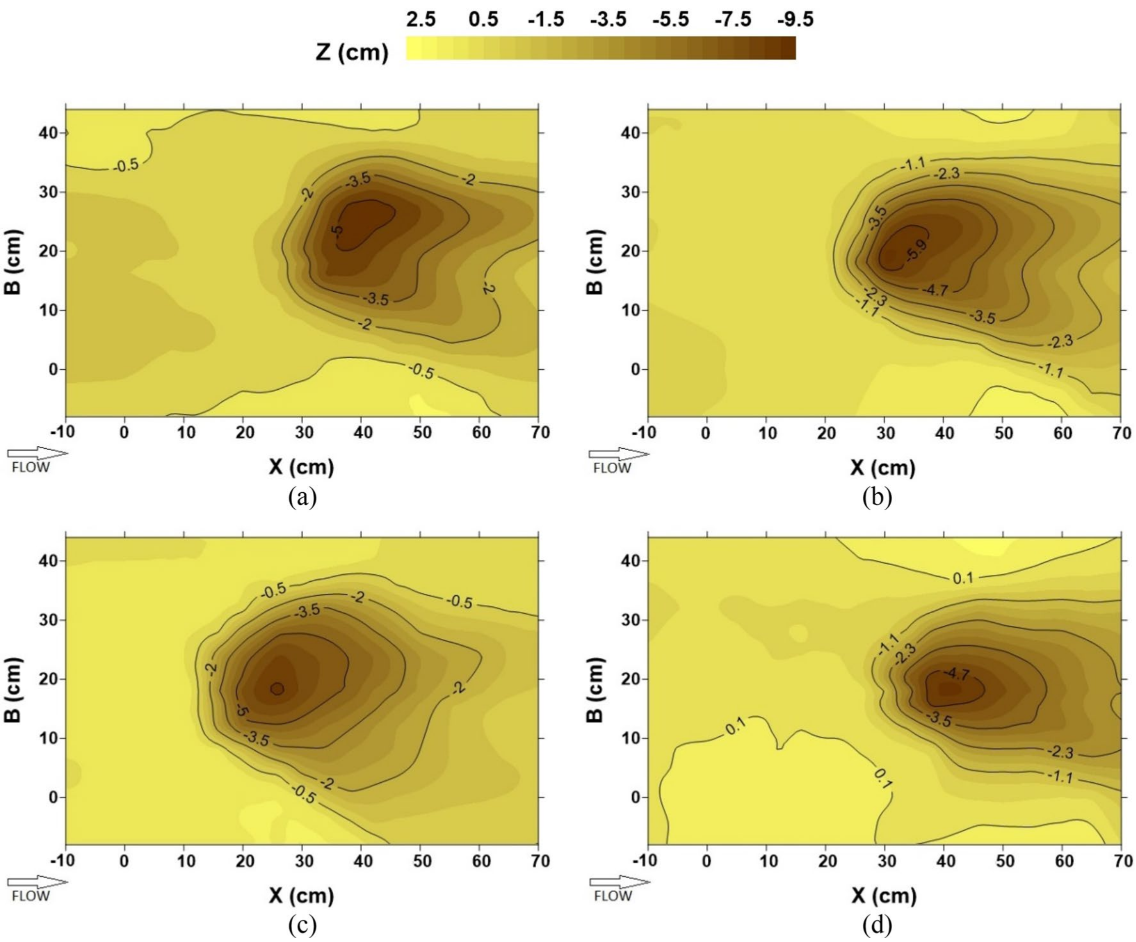

Fig. 6 Bed topography around pit B for *L*/*y* = **a** 8; **b** 12; **c** 16; **d** 0 (single pit)

Table 5 Infilling volume of pits A and B

Pit type	Infilling volume) %)		
	$L/y=8$	$L/y=12$	$L/y=16$
Pit A	89.02	88.79	87.47
Pit B	64.94	59.03	52.08

and then, using the obtained results, the appropriate shape for the mining pit was selected. All numerical simulations featured $d_{50}/y=0.016$, $H/y=1.59$, and $U/U_c=1.2$.

For $l/b=0.59$, the pit fills completely, and the pit bed elevation is approximately equal to the upstream bed level. However, For $l/b=1.68$, the maximum depth of the pit is comparable with the pit depth at the beginning of the simulation (Fig. 14). Hence, one can conclude that due to the replenishment process, the pit bed elevation increases by decreasing the ratio of pit length to its width (pit shape extension in spanwise direction).

The velocity of nick point migration (U_m) is the index of the infilling volume rate of the pit. From Fig. 15, the pit infilling rate in the diffusion (second) period is around two-to-three times greater than that of the convection (first) period. Therefore, the diffusion period has an important role in the infilling process as it increases the bed elevation of the mining pit. It can be also found that by decreasing l/b (smaller distances between the upstream and downstream slopes of the pit), the convection period diminishes, which may lead to an increase in the pit infilling volume (or a decrease in the pit depth). The effects of pit plan shape on infilling volume are presented in Fig. 16, which shows that the pit infilling volume decreases by 30% when l/b increases from 0.78 to 1.68. In addition, for $l/b<1.2$, the pit fills completely, and its plan shape does not have significant effects on the infilling volume.

Effects of distance between pits

The effects of distance between pits have been investigated by Haghnazar and Saneie (2019) for $l/b=1.28$. However, in the present study, numerical simulations are conducted to evaluate the effect of this parameter for different pit shapes

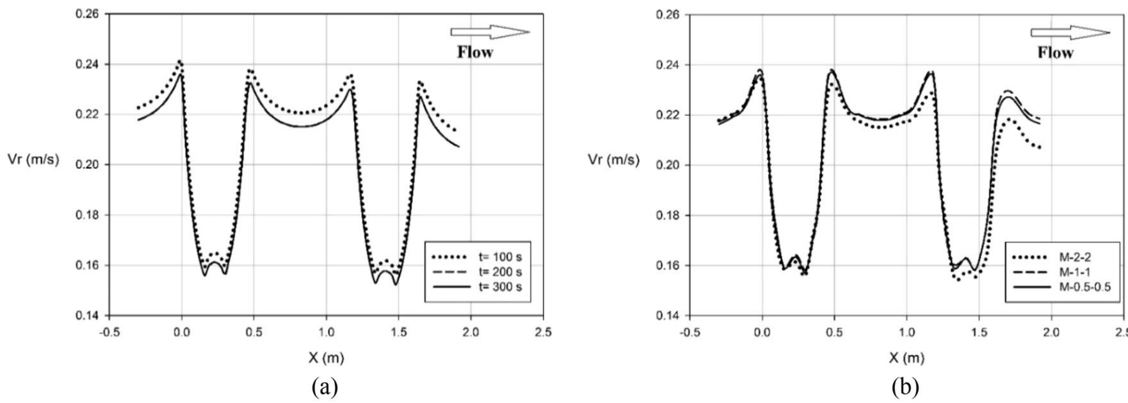

Fig. 7 Variation of the mean flow velocity with: **a** time duration of the numerical simulation; **b** mesh sizes

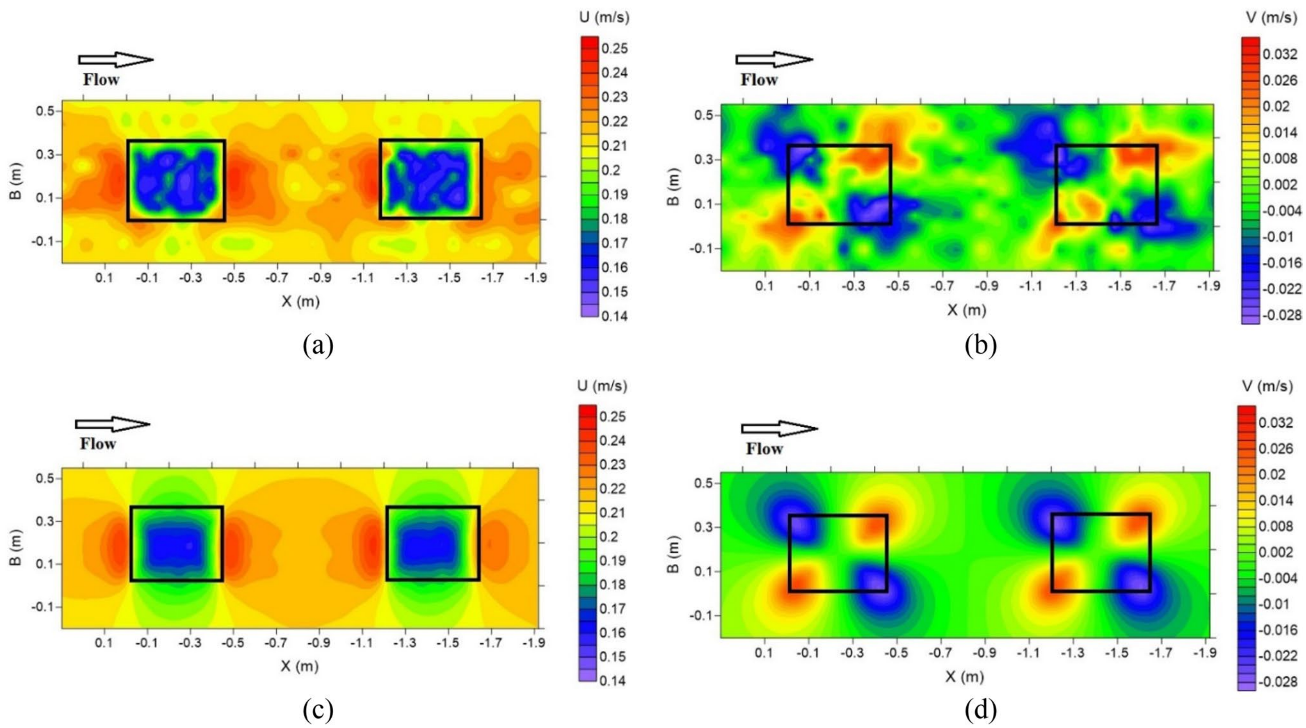

Fig. 8 Results of the velocity contours: **a** laboratory results of streamwise velocity component; **b** laboratory results of spanwise velocity component; **c** numerical results of streamwise velocity component; **d** numerical results of spanwise velocity component

in the range $0.59 \le l/b \le 1.28$, over which there is a high efficiency for replenishment of river mining pits (mentioned in the previous section). According to the experimental results, the distance between the pits has no significant influence on the infilling volume of pit A, while pit B receives less sediment at higher L/y values. As shown in Table 7, by considering different values for L/y and l/b, the interaction between these two parameters is evaluated in this section. For each l/b set, the parameter L/y was studied in a range, beyond which the pits behave separately (having no interaction on each other). In addition, all numerical simulations featured $d_{50}/y = 0.016$, $H/y = 1.59$, and $U/U_c = 1.2$.

Figure 17 shows the variations of pit B infilling volume with respect to L/y for different values of l/b. From this figure, when $l/b = 1.28$, by increasing the distance between the pits, the infilling volume of pit B diminishes to a minimum value occurred at $L/y = 16 \sim 20$. Then, it increases to reach the infilling volume of the single pit at $L/y \approx 32$. For $l/b = 0.78$ and 0.59, the downstream pit infilling volume is

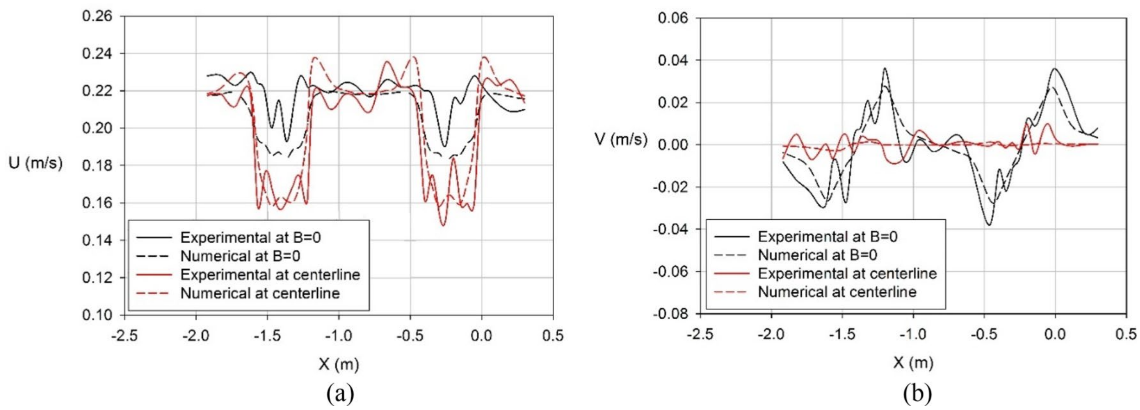

Fig. 9 Variation of the mean velocity in different longitudinal sections: **a** streamwise component; **b** spanwise component

Table 6 Accuracy of the sediment transport model to simulate the infilling volume

Sediment transport capacity equations	Estimated values (%)	Measured value (%)
Wu et al.'s (2000) formula	62.00	52.08
Modified Ackers and White's formula (Proffitt and Sutherland 1983)	67.05	
SEDTRA module (Garbrecht et al. 1995)	74.66	
Modified Engelund and Hansen's formula (Wu and Vieira 2000)	70.10	

a monotonic increasing function of L/y, and it reaches the single pit infilling volume at $L/y = 20$ and 16, respectively. According to economic considerations, the smaller distance between the pits is more feasible. Hence, it can be concluded that smaller l/b values are more cost-effective if $l/b < 1$. This is because the slope of the infilling volume curve is steeper for smaller values of l/b; that is, due to the smaller distance between the upstream and downstream slopes, the pits with a wider opening in the spanwise direction are more cost-effective. In the studied domain, the downstream pit infilling volume is least for $l/b = 1.28$ and $L/y = 16$–20, and it is maximum for $l/b = 0.59$ and $L/y = 16$. According to the results, the best infilling of the downstream pit occurs in following conditions:

$$\begin{cases} L/y > 16 \text{ if } \quad l/b < 0.8 \\ L/y > 28 \text{ if } 0.8 \le l/b < 1 \\ L/y > 32 \text{ if } \quad l/b \ge 1 \end{cases} \tag{13}$$

Effects of pit depth

From the previous section, the minimum infilling volume occurs when $l/b = 1.28$ and $L/y = 16$–20. In the current section, three simulations (having $H/y = 1.25$, 1.42, and 1.59) were conducted to evaluate the pit depth effects ($l/b = 1.28$, $L/y = 16$, $U/U_c = 1.2$, and $d_{50}/y = 0.016$). In these simulations, the dimensions of the pit surface and bottom were kept constant. Pit A was completely filled in all conducted simulations ($H \le 9.5$ cm or $H/y \le 1.59$), in which the pit upstream slope has reached its downstream slope, thereby accelerating the infilling process, but the variations in the pit bottom elevation are not significant. This leads to a slight increase in the infilling volume.

Figure 18 demonstrates the effects of H/y on the infilling volume of pit B. From this figure, by decreasing the depth of pit B from $H/y = 1.59$ to $H/y = 1.25$, its infilling volume increases up to 20%. Through extrapolating the infilling volume data, it may be concluded that pit B fills in $H/y = 0.7$ completely.

Effects of the sediment size

Considering $d_{50}/ = 0.01$, 0.013, and 0.016, the sediment size effects were studied by conducting three numerical simulations, in which $l/b = 1.28$, $L/y = 16$, $U/U_c = 1.2$, and $H/y = 1.59$. It should be noted that different critical velocities are needed for mobilizing various bed sediment sizes. By decreasing d_{50}/y in the three simulations, the flow discharge was reduced to get a constant U/U_c value ($= 1.2$).

Figure 19a shows the effects of d_{50}/y on the longitudinal bed profile in pit B centerline. By decreasing the sediment size, the migration and the downstream erosion of pit B

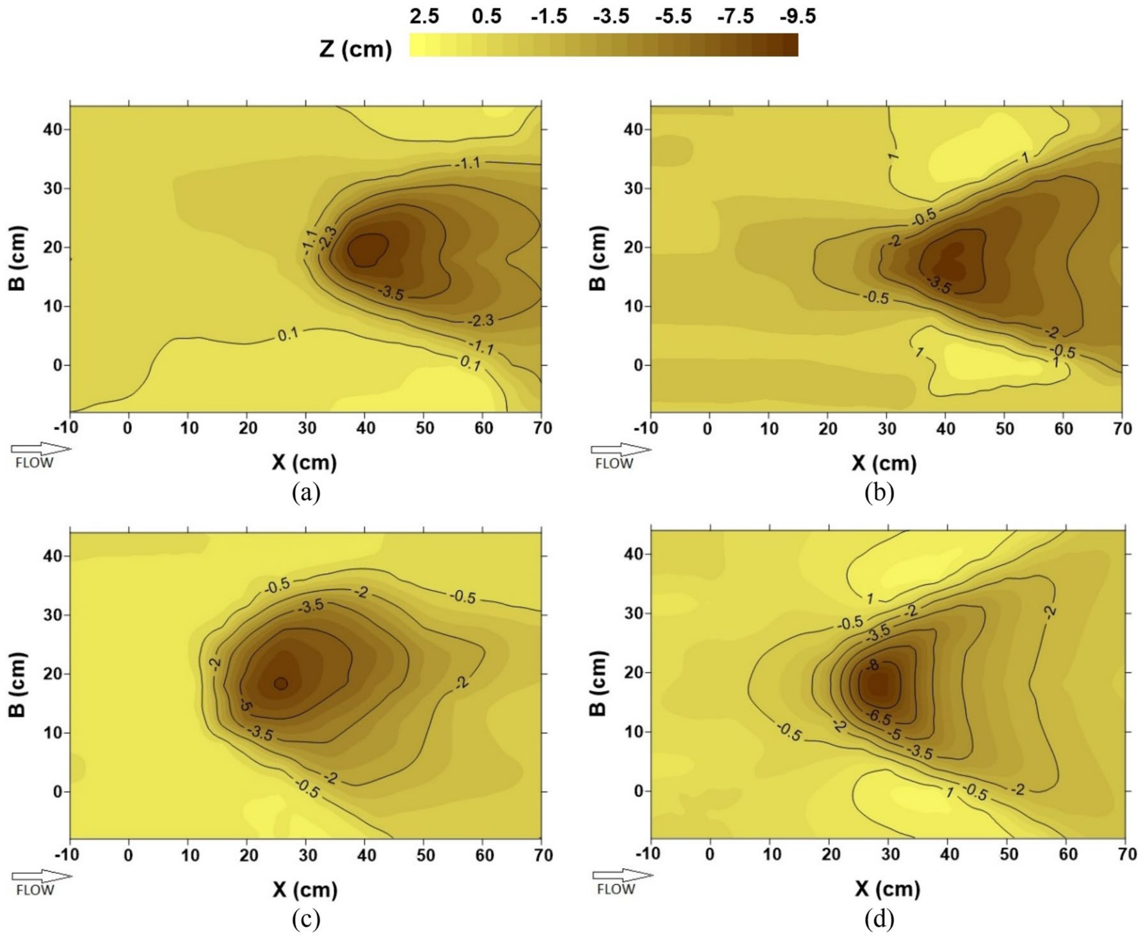

Fig. 10 Bed topography around: **a** pit A-laboratory results; **b** pit A-numerical results; **c** pit B-laboratory results; **d** pit B-numerical results

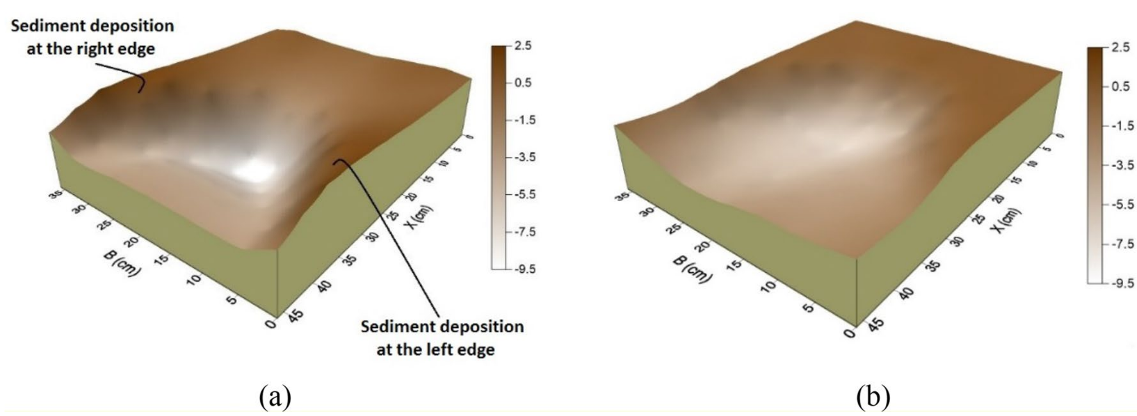

Fig. 11 Comparison of the pit infilling between: **a** numerical simulation; and **b** experimental measurements

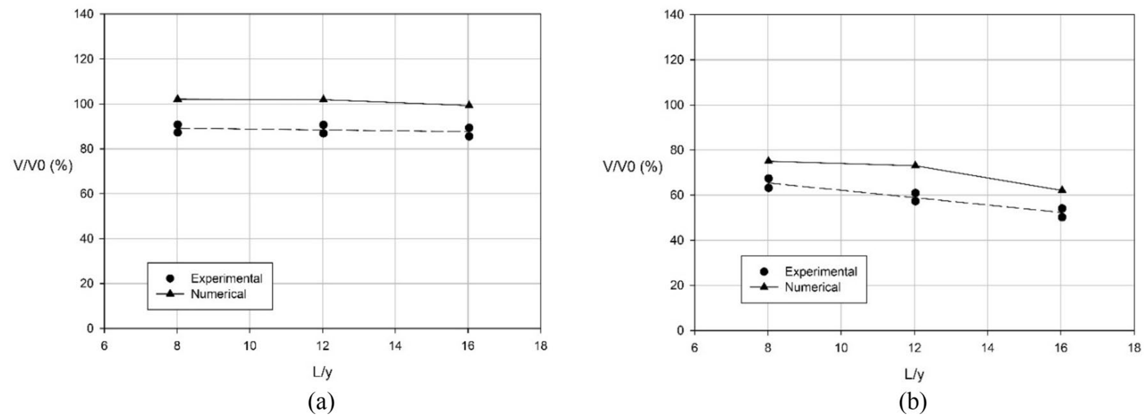

Fig. 12 Infilling volume of the mining pits for $l/b = 1.28$: **a** pit A; **b** pit B

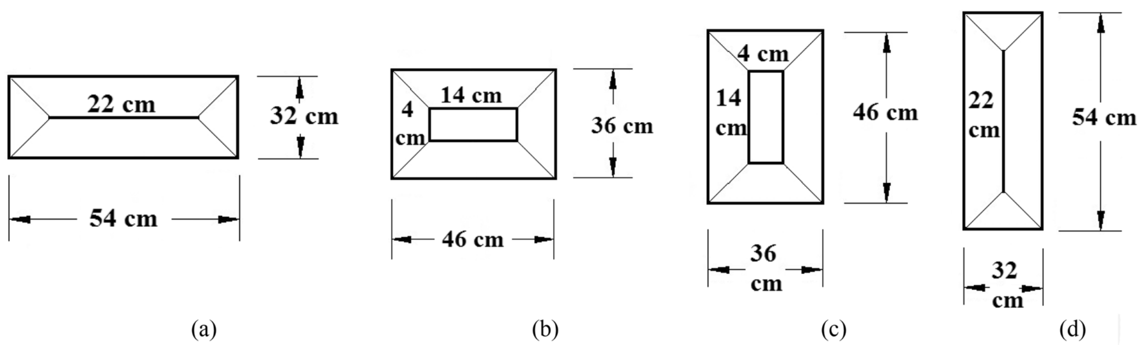

Fig. 13 Different plan shapes of the mining pits with $l/b =$ **a** 1.68; **b** 1.28; **c** 0.78; **d** 0.59

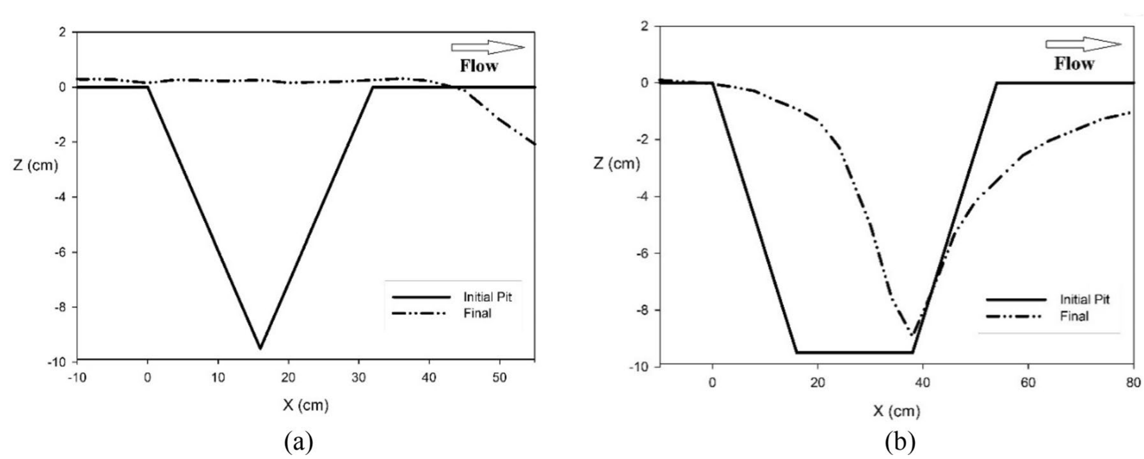

Fig. 14 Longitudinal bed profiles in the mining pit centerline for $l/b =$ **a** 0.59; and **b** 1.68

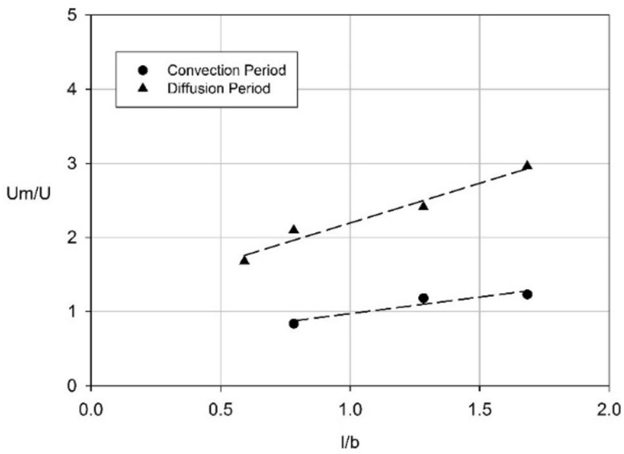

Fig. 15 Variation of the nick point migration velocity in diffusion and convection periods (single pit)

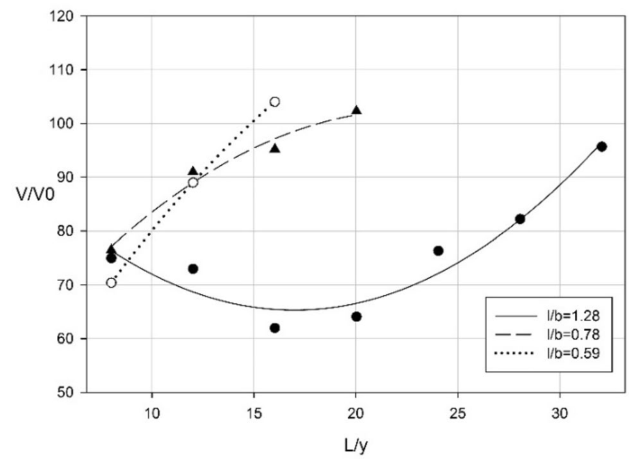

Fig. 17 Variation of the infilling volume with the distance between the pits (*L*/*y*)

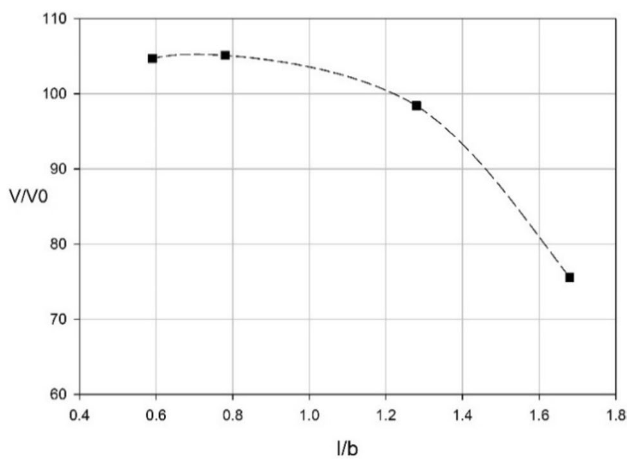

Fig. 16 Variation of the infilling volume with plan shape (*l*/*b*) for the single pit

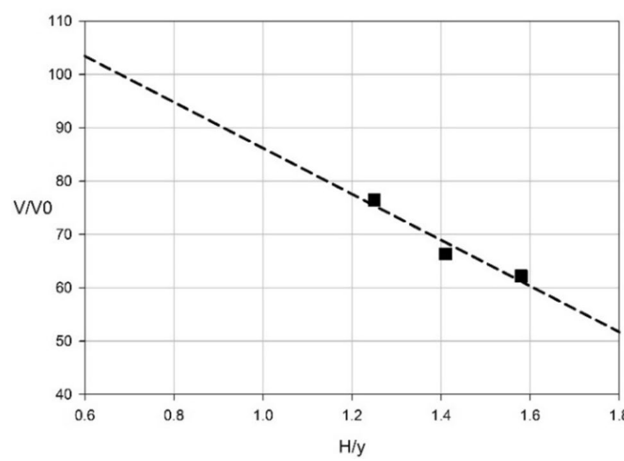

Fig. 18 Variation of the infilling volume with *H*/*y* for pit B

Table 7 Details of the numerical simulations to study the effect of the distance between the pits

Run no.	*L*/*y*	*l*/*b*
1	8	0.59
2	12	0.59
3	16	0.59
4	8	0.78
5	12	0.78
6	16	0.78
7	20	0.78
8	8	1.28
9	12	1.28
10	16	1.28
11	20	1.28
12	24	1.28
13	28	1.28
14	32	1.28

intensify. Figure 19b indicates d_{50}/y effects on its infilling volume. As shown, by increasing d_{50}/y from 0.01 to 0.016, the infilling volume slightly decreases (about 8%).

Effects of the approaching flow velocity

The effects of approaching flow velocity on the longitudinal bed profile and the infilling volume are evaluated considering different values of $U/U_c = 1.15$, 1.2, and 1.25 when $l/b = 1.28$, $L/y = 16$, $d_{50}/y = 0.016$, and $H/y = 1.59$. Figure 20a, b shows U/U_c effects on the longitudinal bed profile in pit B centerline and its infilling volume, respectively. By

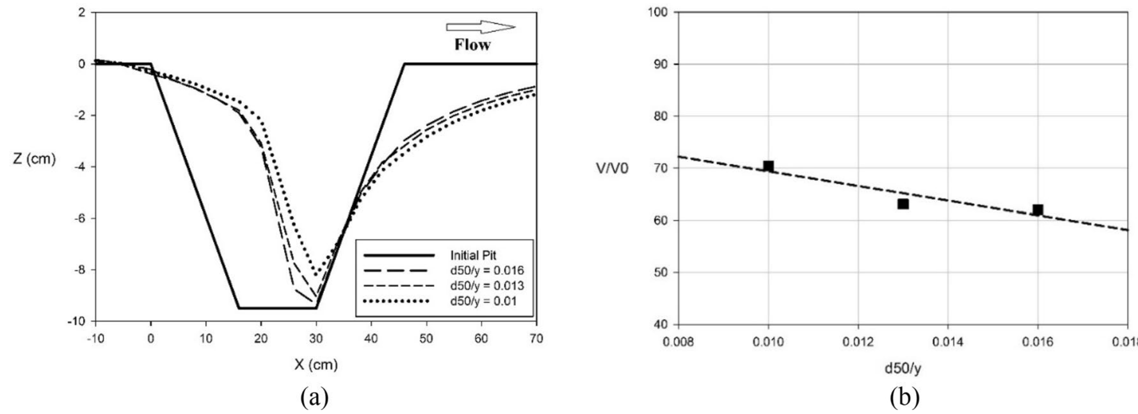

Fig. 19 Effects of d_{50}/y on: **a** longitudinal bed profile and **b** infilling volume of pit B

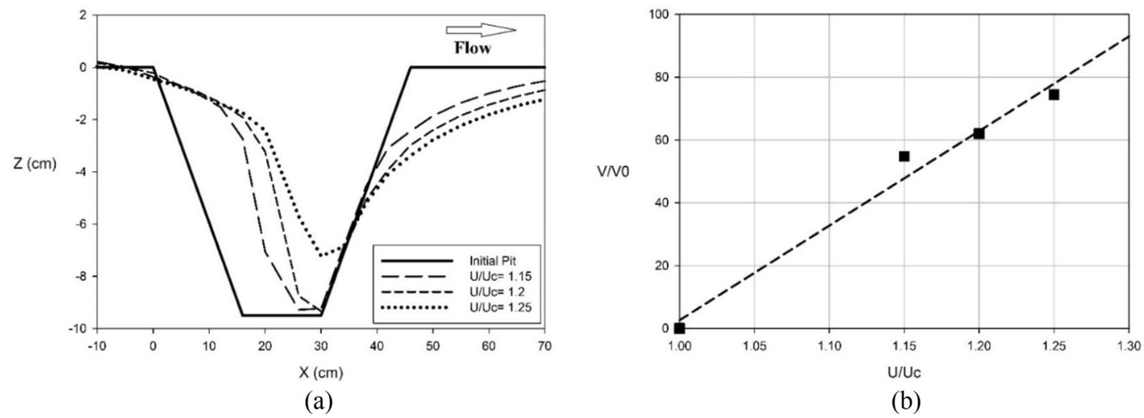

Fig. 20 Effects of U/U_c on: **a** longitudinal bed profile and **b** infilling volume of pit B

increasing U/U_c, both migration and infilling volume of pit B increase. As shown, the infilling volume increases by 20% when U/U_c increases from 1.15 to 1.25. In this trend, the pit experiences the diffusion period, which has a high infilling rate (shown in Fig. 15).

Application

Figures 21 and 22 show the illustrative diagrams to demonstrate the effects of various parameters on infilling of upstream and downstream pits, and propose guidelines for their better replenishment. The important parameters in selecting the upstream pit location are the sediment size, the approaching flow velocity, the pit depth, and its plan shape. The distance between pits is the main parameter in choosing the location of downstream pit. The applicability of the diagrams are limited to the mentioned conditions in Table 8.

Conclusions

In this study, the effects of different parameters [including the ratio of distance between pits to approaching flow depth (L/y), the ratio of pit length to its width (l/b), the ratio of pit depth to approaching flow depth (H/y), the ratio of median sediment size to approaching flow depth (d_{50}/y), and the ratio of approaching flow velocity to the sediment critical velocity (U/U_c)] on the mining pit characteristics (i.e., infilling volume, longitudinal bed profile, and bed topography) were investigated using both experimental and numerical (CCHE2D) models.

The obtained bed topography show that the distance from the downstream pit (pit B) does not have a significant effect on the infilling volume of the upstream pit (pit A). However, by increasing the distance between the pits, the infilling volume of pit B decreases. By extending the pits in the spanwise direction, the infilling volume of pit B enhances. A 50% decrease in l/b causes a 30% increase in pit B infilling volume. The results also indicate that the river mining pits

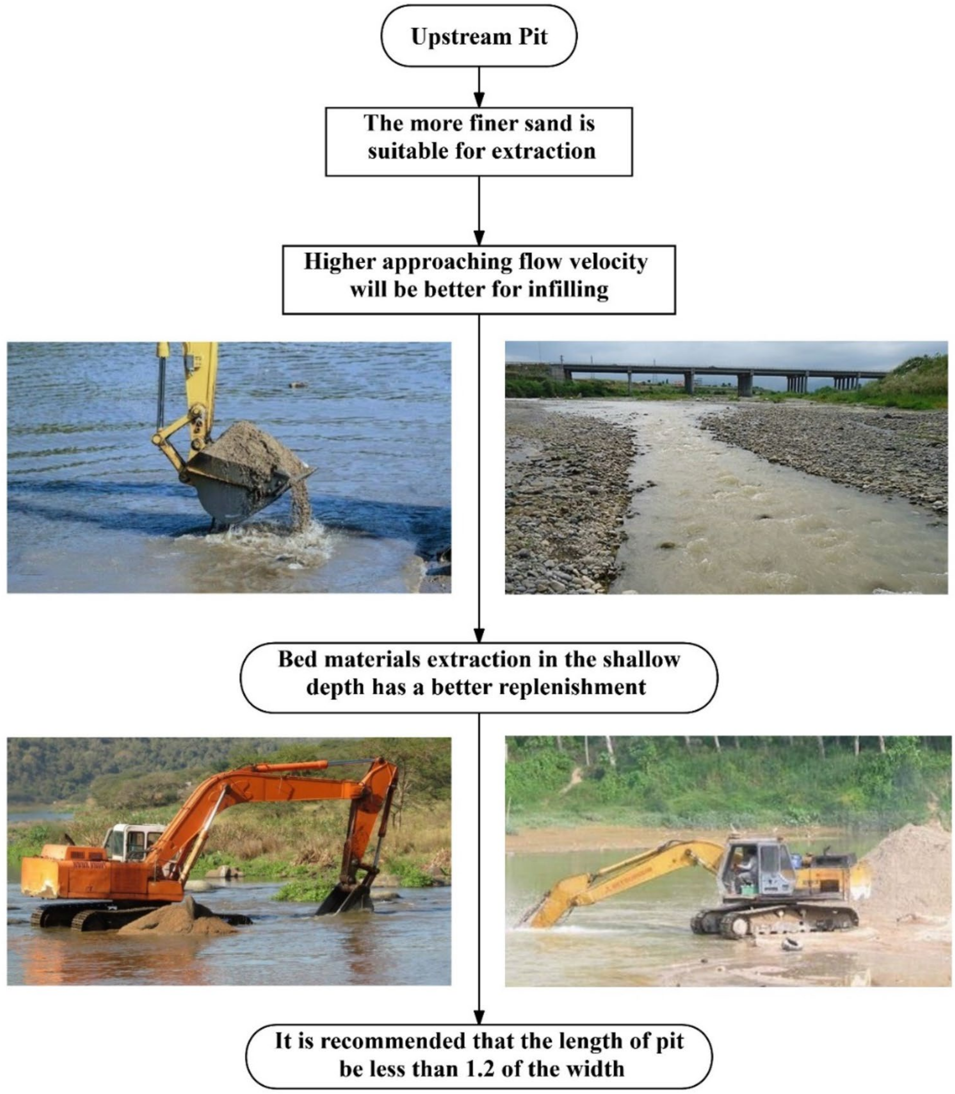

Fig. 21 Diagram guidelines for better infilling of upstream pit (Photos from www.magzter.com)

completely fill when $l/b \leq 1.2$, and the plan shape effects can be neglected.

The effect of the pit distance on the infilling volume depends on the plan shape. For $l/b = 1.28$, by increasing L/y, the infilling volume of pit B decreases and records a minimum value at $L/y = 16$-20; then, it increases and reaches the infilling volume of a single pit at $L/y = 32$. For $l/b < 1$, the infilling volume of pit B monotonically increases with the pit distance, and it reaches the infilling volume of a single pit at $L/y = 20$ and 16 when $l/b = 0.78$ and 0.59, respectively. By increasing the ratio of pit length to its width (pit shape extension in streamwise direction), the pit infilling volume decreases. A pit with smaller depth can be implemented as an alternative to improve the infilling volume.

According to the results of this study, a 20% decrease in the pit depth increases the infilling volume of pit B up to 20%. For a complete pit infilling, it is recommended that the pit depth should be less than 70% of the approaching flow depth. In addition, a decrease in sediment size slightly increases the pit volume infilling. The longitudinal bed profiles show that the migration and the downstream erosion of pit B intensify with the sediment size reduction. However, U/U_c has a considerable effect on the pit infilling volume as the increase of U/U_c from 1.15 to 1.25 causes a 20% enhancement in this parameter, while the pit experiences the diffusion period. Based on the present study limitations, some guidelines are provided for more (or faster) replenishment of river mining pits. Although more data are needed to ensure the generality of these guidelines in different conditions, they can be considered as a first-order approximation in river mining projects.

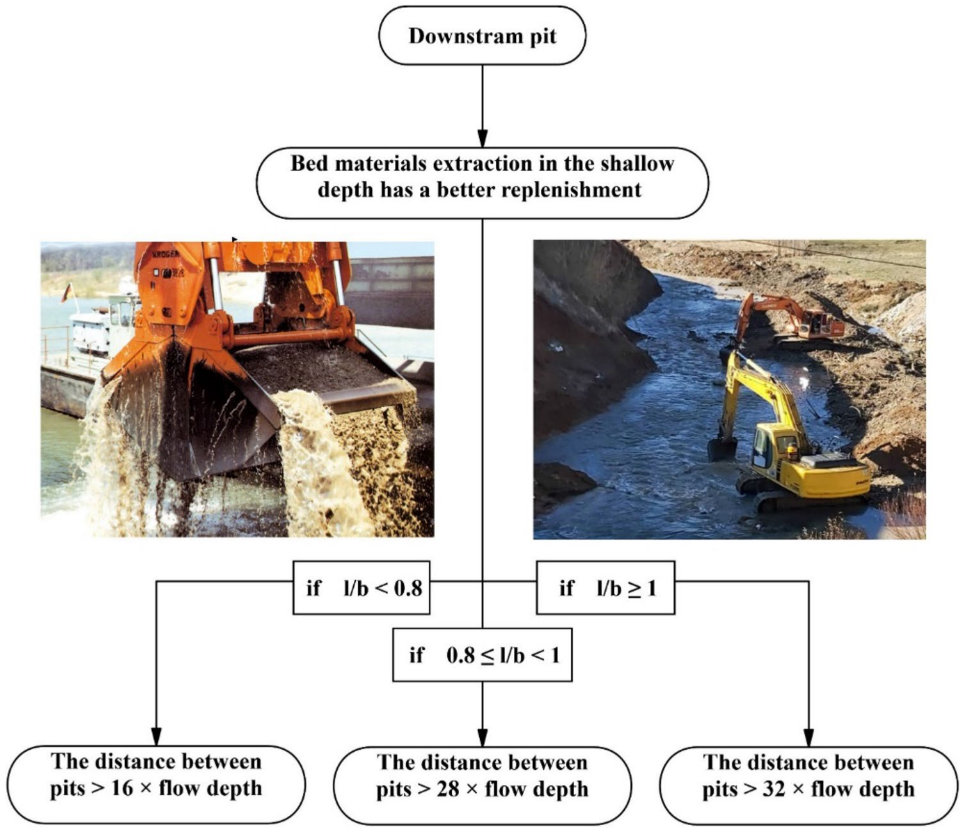

Fig. 22 Diagram guidelines for better infilling of downstream pit (Photos from www.kroeger-greifertechnik.de)

Table 8 Limitations of present study

Parameter	L/y	l/b	H/y	d_{50}/y	U/U_c
Range	8–32	0.59–1.68	1.25–1.59	0.01–0.016	1.15–1.25

References

Ambak MA, Zakaria MZ (2010) Freshwater fish diversity in Sungai Kelantan. J Sustain Sci Manag 5(1):13–20

Ashraf MA, Jamil MM, Yusoff I, Wajid A, Mahmood K (2011) Sand mining effects, causes and concerns: a case study from Bestari Jaya, Selangor, Peninsular Malaysia. Sci Res Essays 6(6):1216–1231

Barman B, Sharma A, Kumar B, Sarma AK (2017) Multiscale characterization of migrating sand wave in mining induced alluvial channel. Ecol Eng 102:199–206

Barman B, Kumar B, Sarma AK (2018) Turbulent flow structures and geomorphic characteristics of a mining affected alluvial channel. Earth Surf Proc Land 43(9):1811–1824

Batalla RJ (2003) Sediment deficit in rivers caused by dams and instream gravel mining. A review with examples from NE Spain. Cuaternario y Geomorfología 17(2):79–91

Bayram A, Önsoy H (2015) Sand and gravel mining impact on the surface water quality: a case study from the city of Tirebolu (Giresun Province, NE Turkey). Environ Earth Sci 73(5):1997–2011

Calle M, Alho P, Benito G (2017) Channel dynamics and geomorphic resilience in an ephemeral Mediterranean river affected by gravel mining. Geomorphology 285:333–346

Chen D (2011) Modeling channel response to instream gravel mining. Desert Research Institute, Las Vegas

Chen D, Liu M (2009) One-and two-dimensional modeling of deep gravel mining in the Rio Salado. World Environmental and Water Resources Congress, Kansas City

Chen D, Acharya K, Stone M (2010) Sensitivity analysis of nonequilibrium adaptation parameters for modeling mining-pit migration. J Hydraul Eng 136(10):806–811

Collins BD, Dunne T (1989) Gravel transport, gravel harvesting, and channel-bed degradation in rivers draining the southern Olympic Mountains, Washington, USA. Environ Geol Water Sci 13(3):213–224

Erskine WD (1990) Environmental impacts of sand and gravel extraction on river systems. The Brisbane River. Australian Littoral Society, Moorooka

Erskine WD, Geary PM, Outhet DN (1985) Potential impacts of sand and gravel extraction on the Hunter River, New South Wales. Aust Geogr Stud 23(1):71–86

Ferguson RI, Church M, Rennie CD, Venditti JG (2015) Reconstructing a sediment pulse: modeling the effect of placer mining on Fraser River, Canada. J Geophys Res Earth Surf 120(7):1436–1454

Garbrecht J, Kuhnle R, Alonso C (1995) A sediment transport capacity formulation for application to large channel networks. J Soil Water Conserv 50(5):527–529

Haghnazar H, Saneie M (2019) Impacts of pit distance and location on river sand mining management. Model Earth Syst Environ 5(4):1463–1472

Jang C, Shimizu Y, Lee GH (2015) Numerical simulation of the fluvial processes in the channels by sediment mining. KSCE J Civ Eng 19(3):771–778

Kondolf GM (1997) PROFILE: hungry water: effects of dams and gravel mining on river channels. Environ Manag 21(4):533–551

Lee HY, Fu DT, Song MH (1993) Migration of rectangular mining pit composed of uniform sediment. J Hydraul Eng 119(1):64–80

Li J, Qi M, Jin Y (2013) Experimental and numerical investigation of riverbed evolution in post-damaged conditions. In: The 35th World Congress of the International Association for Hydro-Environment Engineering and Research. Chengdu, Sichuan, China, pp 4798–4809

Marston RA, Bravard JP, Green T (2003) Impacts of reforestation and gravel mining on the Malnant River, Haute-Savoie, French Alps. Geomorphology 55:65–74

Padmalal D, Maya K (2014) Sand mining: environmental impacts and selected case studies. Springer, Berlin

Padmalal D, Maya K, Sreebha S, Sreeja R (2008) Environmental effects of river sand mining: a case from the river catchments of Vembanad lake, Southwest coast of India. Environ Geol 54:879–889

Papanicolaou ATN, Elhakeem M, Krallis G, Prakash S, Edinger J (2008) Sediment transport modeling review—current and future developments. J Hydraul Eng 134(1):1–14

Plesiński K, Radecki-Pawlik A, Wyżga B (2015) Sediment transport processes related to the operation of a rapid hydraulic structure (Boulder Ramp) in a Mountain Stream Channel: a polish carpathian example. In: Heininger P, Cullmann J (eds) Sediment matters. Springer, Cham, pp 39–58

Proffitt GT, Sutherland AJ (1983) Transport of non-uniform sediments. J Hydraul Res 21(1):33–43

Rinaldi M (2003) Recent channel adjustments in alluvial rivers of Tuscany, Central Italy. Earth Surface Processes and Landforms. J Br Geomorphol Res Group 28(6):587–608

Rinaldi M, Simon A (1998) Bed-level adjustments in the Arno River, central Italy. Geomorphology 22(1):57–71

Salehi Neishabouri SAA, Farhadzadeh A, Amini A (2002) Experimental and field study on mining–pit migration. Int J Sediment Res 17(4):323–331

Sangsefidi Y, MacVicar B, Ghodsian M, Mehraein M, Torabi M, Savage BM (2019) Evaluation of flow characteristics in labyrinth weirs using response surface methodology. Flow Meas Instrum 69:101617

Sangsefidi Y, Torabi M, Tavakol-Davani H (2020) Discussion on "Laboratory investigation of the discharge coefficient of flow in arced labyrinth weirs with triangular plans" by Monjezi et al. (2018). Flow Meas Instrum 72:101709

Scott SH, Jia Y (2005) Simulation of sediment transport and channel morphology change in large river systems. US–China workshop on advanced computational modeling in hydro science and engineering. The University of Mississippi, Oxford, Mississippi, USA, pp 1–11

Sreebha S, Padmalal D (2011) Environmental impact assessment of sand mining from the small catchment rivers in the southwestern coast of India: a case study. Environ Manag 47(1):130–140

Strickler A (1923). (Roesgan, T., and Brownie, W. R., trans. 1981) Contributions to the Question of a Velocity Formula and Roughness Data for Streams, Channels and Closed Pipelines. Pasadena: W. M. Keck Lab of Hydraulics and Water Resources, California Institute of Technology

Sunilkumar R (2002) Impact of sand mining on benthic fauna: a case study from Achankovil river—an overview. Catholicate College, Pathanamthitta, p 38

Surian N, Rinaldi M (2003) Morphological response to river engineering and management in alluvial channels in Italy. Geomorphology 50(4):307–326

Wu W (2001) "CCHE2D Sediment Transport Model" Technical Report No. NCCHE-TR-2001-3, School of Engineering, The University of Mississippi

Wu W, Vieira DA (2002) One-dimensional channel network model CCHE1D version 3.0–technical manual. National Center for Computational Hydroscience and Engineering Technical Report No. NCCHE-TR-2002-02

Wu W, Wang SS, Jia Y (2000) Nonuniform sediment transport in alluvial rivers. J Hydraul Res 38(6):427–434

Yuill BT, Gaweesh A, Allison MA, Meselhe EA (2016) Morphodynamic evolution of a lower Mississippi River channel bar after sand mining. Earth Surf Proc Land 41(4):526–542

Zhang Y (2005) CCHE2D-GUI–graphical user interface for the CCHE2D model user's manual–version 2.2. National Center for Computational Hydroscience and Engineering, Mississippi, USA